Comparative analysis of statistical methods for landslide susceptibility mapping in the Bostanlik District, Uzbekistan

Mukhiddin Juliev [a,*], Martin Mergili [b,c], Ismail Mondal [d], Bakhtiar Nurtaev [e], Alim Pulatov [f], Johannes Hübl [a]

[a] University of Natural Resources and Life Sciences (BOKU), Institute of Mountain Risk Engineering, Vienna, Austria
[b] University of Natural Resources and Life Sciences (BOKU), Institute of Applied Geology, Vienna, Austria
[c] University of Vienna, Department of Geography and Regional Research, Vienna, Austria
[d] Department of Marine Science, University of Calcutta, India
[e] Institute of Geology and Geophysics, State Committee on Geology and Mineral Resources of Uzbekistan, Tashkent, Uzbekistan
[f] EcoGIS Center, Tashkent Institute of Irrigation and Agricultural Mechanization Engineers, Uzbekistan

HIGHLIGHTS

- The present study is the first attempt of a statistical landslide susceptibility analysis for part of the territory of Uzbekistan.
- Statistical index (SI), frequency ratio (FR) and certainty factor (CF) are employed for the landslide susceptibility mapping.
- The statistical index method results in the best model performance.
- The landslide-predictor relationships confirm findings of previous studies.
- The results perform slightly better than those obtained in some previous studies, possibly due to the polygon-based inventory used.

GRAPHICAL ABSTRACT
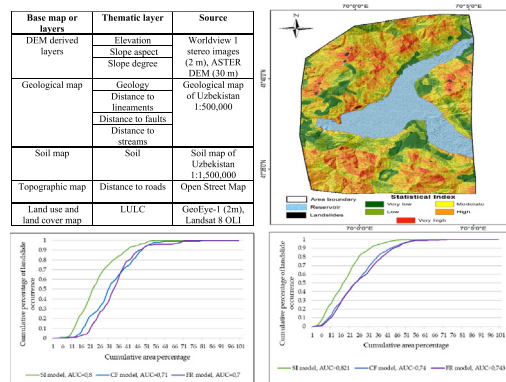
ABSTRACT

The Bostanlik district, Uzbekistan, is characterized by mountainous terrain susceptible to landslides. The present study aims at creating a statistically derived landslide susceptibility map – the first of its type for Uzbekistan - for part of the area in order to inform risk management. Statistical index (SI), frequency ratio (FR) and certainty factor (CF) are employed and compared for this purpose. Ten predictor layers are used for the analysis, including geology, soil, land use and land cover, slope, aspect, elevation, distance to lineaments, distance to faults, distance to roads, and distance to streams. 170 landslide polygons are mapped based on GeoEye-1 and Google Earth imagery. 119 (70%) out of them are randomly selected and used for the training of the methods, whereas 51 (30%) are retained for the evaluation of the results. The three landslide susceptibility maps are split into five classes, i.e. very low, low, moderate, high, and very high. The evaluation of the results obtained builds on the area under the success rate and prediction rate curves (AUC). The training accuracies are 82.1%, 74.3% and 74%, while the prediction accuracies are 80%, 70% and 71%, for the SI, FR and CF methods, respectively. The spatial relationships between the landslides and the predictor layers confirmed the results of previous studies conducted in other areas, whereas model performance was slightly higher than in some earlier studies – possibly a benefit of the polygon-based landslide inventory used.

© 2018 Elsevier B.V. All rights reserved.

* Corresponding author.
E-mail address: mukhiddin.juliev@students.boku.ac.at (M. Juliev).

1. Introduction

Landslides are common hazardous processes, which frequently cause loss of life and property in mountainous and hilly areas all around the world (Gutiérrez et al., 2015; Chen et al., 2018; Hong et al., 2018). Besides other types of hazards such as earthquakes, droughts and floods, the territory of Uzbekistan is also prone to landsliding. Based on the research conducted by the Central Asia and Caucasus Disaster Risk Management Initiative (CAC DRMI) from 1988 to 2007, 23% of all recorded natural disasters in Uzbekistan are the consequence of landslide processes. During the past 80 years, 2600 landslide events were documented in Uzbekistan. Around 50 people lost their lives during a landslide in the Angren region on 4 May 1991 (CACDRMI, 2009).

The Bostanlik district is one of the most landslide-prone areas of Uzbekistan. Most of the landslides are triggered by earthquakes, snow melting or precipitation, or combinations thereof. The presence of a mountain reservoir increases the frequency of landslide occurrence, in particular for areas near the water body (Juliev et al., 2017). Around 65% of all landslides in Uzbekistan are located in the Tashkent region, which the Bostanlik district forms part of. Consequently, the monitoring of existing landslides is necessary, and landslide susceptibility assessments are highly recommended as a basis to mitigate these hazards.

Landslide hazard and risk assessments start from landslide susceptibility mapping of the territory under investigation (Van Westen et al., 2008; Golovko et al., 2017). Generally, landslide susceptibility is the spatial probability of landsliding in a given area, depending on a combination of various factors such as geology, land use and land cover (LULC), tectonics, slope, aspect, and others (Guzzetti et al., 2006; Wu et al., 2016). During the last decades, a variety of approaches for landslide susceptibility analysis have been developed. They are categorized into heuristic, physically-based and statistical methods (Van Westen, 2002; Bilaşco et al., 2011; Althuwaynee et al., 2012; Devkota et al., 2013; Ozdemir and Altural, 2013; Akbari et al., 2014; Wang et al., 2015; Basharat et al., 2016; Chen et al., 2016; Hussin et al., 2016; Ilia and Tsangaratos, 2016; Zare et al., 2013; Vakhshoori and Zare, 2016; Cui et al., 2017; Fan et al., 2017; Hong et al., 2017).

Few studies on landslide susceptibility mapping in the territory of Central Asia have yet been documented. Saponaro et al. (2015a) conducted research on earthquake-triggered landslide susceptibility, whereas Saponaro et al. (2015b) performed a statistical landslide susceptibility analysis for the entire territory of Kyrgyzstan. Golovko et al. (2017) compared an inventory of landslides automatically detected from satellite data with an inventory derived from mapping by experts.

The main scope of the present study is to derive and to evaluate a landslide susceptibility map for the surroundings of the Charvak Reservoir, a very important touristic site in the Bostanlik district. This work is the first attempt of a statistical landslide susceptibility analysis for part of the territory of Uzbekistan. The main contributions/novelties can be summarized as follows:

- General: by applying the established techniques to a yet unstudied area, the work contributes to increase the robustness of knowledge on the relationship between landslides and possible causative factors.
- Regional: increased knowledge of landslide susceptibility and causative factors in the surroundings of the Charvak Reservoir in the Bostanlik District, Uzbekistan. The results presented shall represent a valuable basis for the government authorities and stakeholders to inform future land use planning and risk mitigation activities.
- Methodical: assessment of the gain of a polygon-based landslide inventory derived from high-resolution satellite data in terms of model performance, compared to a point-based inventory.

2. Materials and methods

2.1. Study area

The Bostanlik district is located in the north-eastern part of Uzbekistan between 41°00′ and 42°20′ North and 69°30′ and 71°20′ East. With a total area of 4982 km², it is the largest district in the Tashkent region. The administrative center is the city of Gazalkent. According to the census of 2000, there were 142,900 people living in the district, whereas according to the census of 2013, about 160,000 people inhabited the area with >60% of the residents living in rural areas. The largest recreation sites of Uzbekistan are located in Bostanlik district.

Almost the entire area is covered by high mountains such as the Western Tien Shan, Karzhantau, Pskem, Ugam and Chatkal. The elevation varies from 568 m to the summit of Adelung at 4301 m asl. Elevation generally increases from west to east and from south to north. The district further belongs to a seismically active zone, resulting in more than eight earthquakes with the different magnitude occurring on average per year. Table 1 shows the relation between the significant Pamir-Hindukush earthquake events and the landslides which occurred thereafter (Niyazov and Nurtaev, 2013).

The area is further characterized by a continental climate: annual mean minimum and maximum, and absolute minimum and maximum temperatures are −9 °C, +21 °C, −26 °C and +46 °C, respectively. The total amount of precipitation measured at the meteorological stations reaches up to 800–1200 mm per year. The main drainage line of the area is the Chirchik River. Within the district, the Charvak Reservoir operates with an area of coverage of 40 km² and with 2 billion m³ of storage volume (Belolipov et al., 2013).

We have selected the surroundings of the Charvak Reservoir, covering an area of approx. 177 km², for the landslide susceptibility analysis (Fig. 1). The dominant landslide types observed in the study area are translational slides, rotational slides, earth flows, debris flows and debris slides, with broadly varying volumes.

2.2. Data preparation

2.2.1. Landslide inventory

Landslide inventories represent an important basis for statistical landslide susceptibility analyses and can be prepared in various ways (Sara et al., 2015). High and very high-resolution optical images from Google Earth are most commonly used in newer studies (Sato and Harp, 2009). In the present study, Google Earth and GeoEye-1 satellite data are employed. 170 landslides are mapped in total. Thereby, one polygon is placed in the central part of each observed landslide scarp. 119 (70%) out of those landslides are used for training and 51 (30%) are retained for the evaluation of the results obtained. Splitting of the inventory follows a random procedure. No distinction between different types of landslides is made in the present study.

Table 1
Pamir Hindukush Earthquakes and landslides occurred in Tashkent Province, Uzbekistan.

| Date	Depth, km	Magnitude	Volume of landslides, mln/m³	Place of occurrence
21.05.1969	217	5.8	0.24	Tashkent Province
06.10.1969	203	5.5	2.0	Tashkent Province
06.10.1969	203	5.5	0.7	Tashkent Province
16.05.1995	189	5.9	25.0	Tashkent Province
20.03.1998	227	6.0	2.0	Tashkent Province
05.04.2004	187	6.6	0.3	Tashkent Province
05.04.2004	187	6.6	50.0	Tashkent Province
03.04.2007	222	6.7	8.0	Tashkent Province
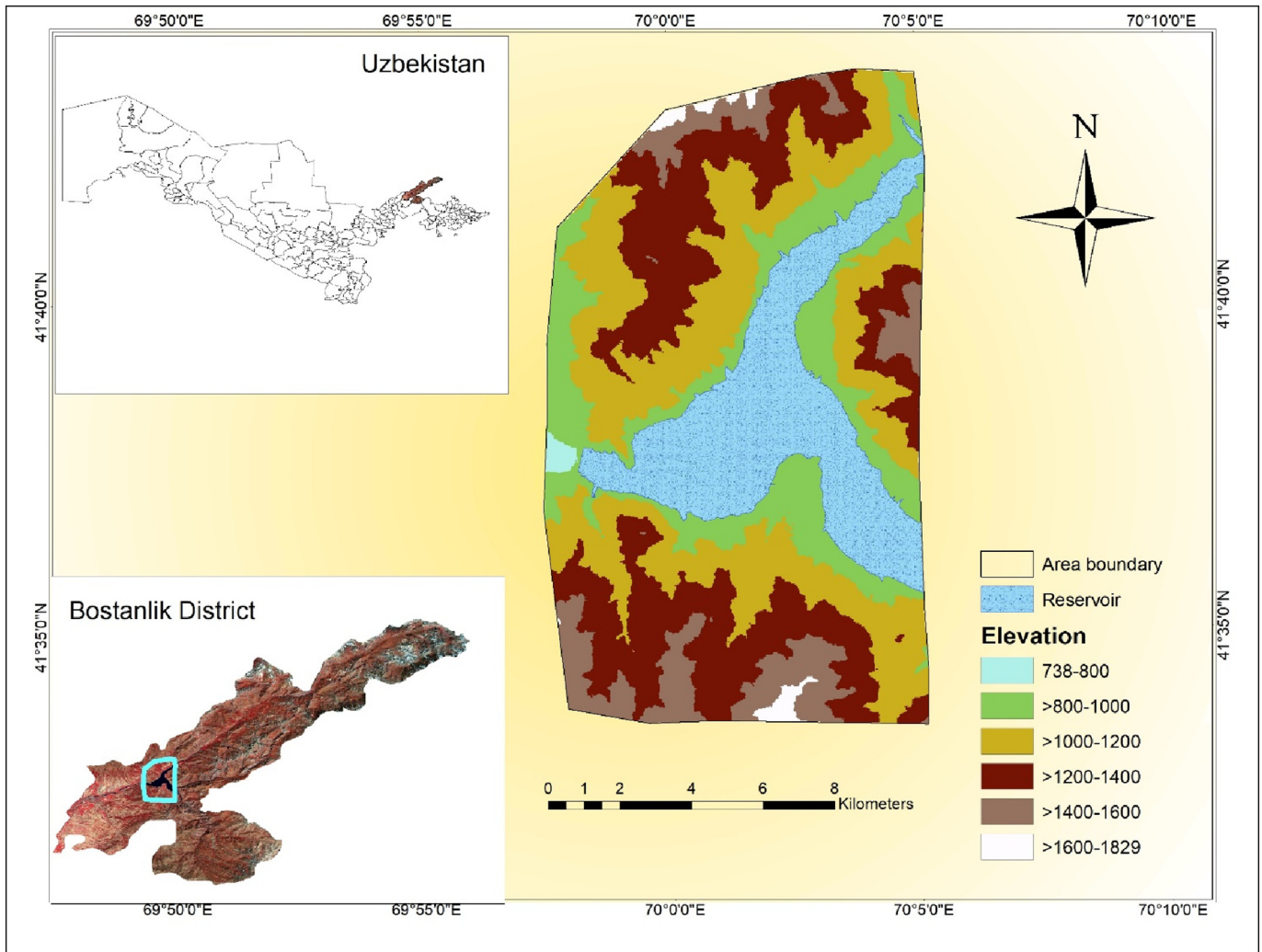
Fig. 1. Location of the study area in the north-eastern part of Uzbekistan.

2.2.2. Predictor layers

The thematic predictor layers for statistical landslide susceptibility analyses are often selected according to the geomorphological characteristics of the study area, the type of landslides and the method employed (Tien Bui et al., 2013; Hong et al., 2017). There is still disagreement whether to constrain the predictor layers to a small number (Akgun, 2012), or to use a large number of layers (Catani et al., 2013;

Meinhardt et al., 2015). The second type of approach is followed in the present study. Ten predictor layers are derived from the digital elevation model (DEM) as well as from the geological, soil, topographic, and land use and land cover (LULC) maps, in order to be used for the landslide susceptibility analysis. The layers are summarized in Table 2.

2.2.2.1. DEM derived layers. Elevation, slope and aspect are the most commonly used DEM parameters for landslide susceptibility mapping (Ercanoglu et al., 2004; Pourghasemi et al., 2012). For our study area, the elevation varies from 738 to 182 m and is divided into six classes with intervals of 200 m (Fig. 2a). Aspect is related to the direction of precipitation, wind and sunlight. It is classified into nine categories: flat, north, northeast, east, southeast, south, southwest, west, northwest (Fig. 2b). The slope values range between 0° and 62° and are grouped into five classes (Fig. 2c).

2.2.2.2. Layers from the geological map. Geology plays a very important role for landslide susceptibility studies because different lithological classes vary among themselves in terms of mechanical and hydraulic characteristics (Pourghasemi et al., 2013; Pourghasemi et al., 2018). The study area is divided into two lithological units: quaternary with an alluvial complex and carboniferous with a carbonate-terrigenous complex. Most of the territory is assigned to the quaternary deposits including sand, gravel, conglomerate and loess. The carbonate-terrigenous complex consists of limestone and dolomite with a bed of siltstone (Fig. 2d). Lineaments as linear features serve as indicators for

Table 2
Sources of the thematic layers.

Base map or layers	Thematic layer	Source
DEM derived layers	Elevation Slope aspect Slope degree	Worldview 1 stereo images (2 m), ASTER DEM (30 m)
Geological map	Geology Distance to lineaments Distance to faults Distance to streams	Geological map of Uzbekistan 1:500,000
Soil map	Soil	Soil map of Uzbekistan 1:1,500,000
Topographic map	Distance to roads	Open street map
Land use and land cover map	LULC	GeoEye-1 (2 m), Landsat 8 OLI

potential tectonic activity (Meten et al., 2015; Teerarungsigul et al., 2016). The distance to lineaments layer is classified into seven equidistant categories, using an interval of 300 m (Fig. 2e). Faults are directly related to the tectonic activity of the region and characterized by the presence of weak and fractured rocks (Chen et al., 2016). The distance to faults layer is divided into seven equidistant classes with intervals
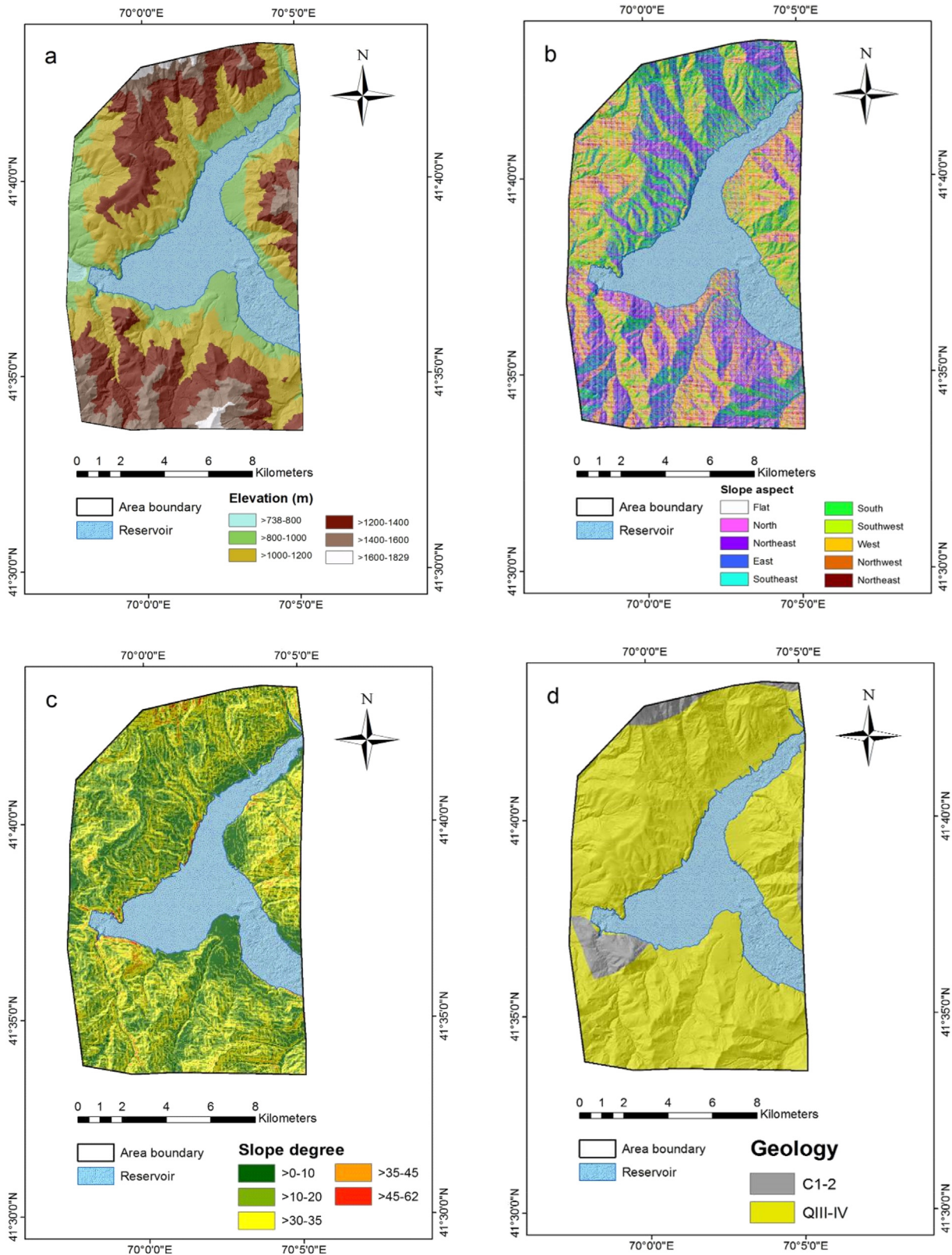

Fig. 2. Predictor layers used for the landslide susceptibility mapping: (a) Elevation, (b) Slope aspect, (c) Slope degree, (d) Geology, (e) Distance to lineaments, (f) Distance to faults, (g) Distance to streams, (h) Soil map, (i) Distance to roads, (j) Land use land cover.
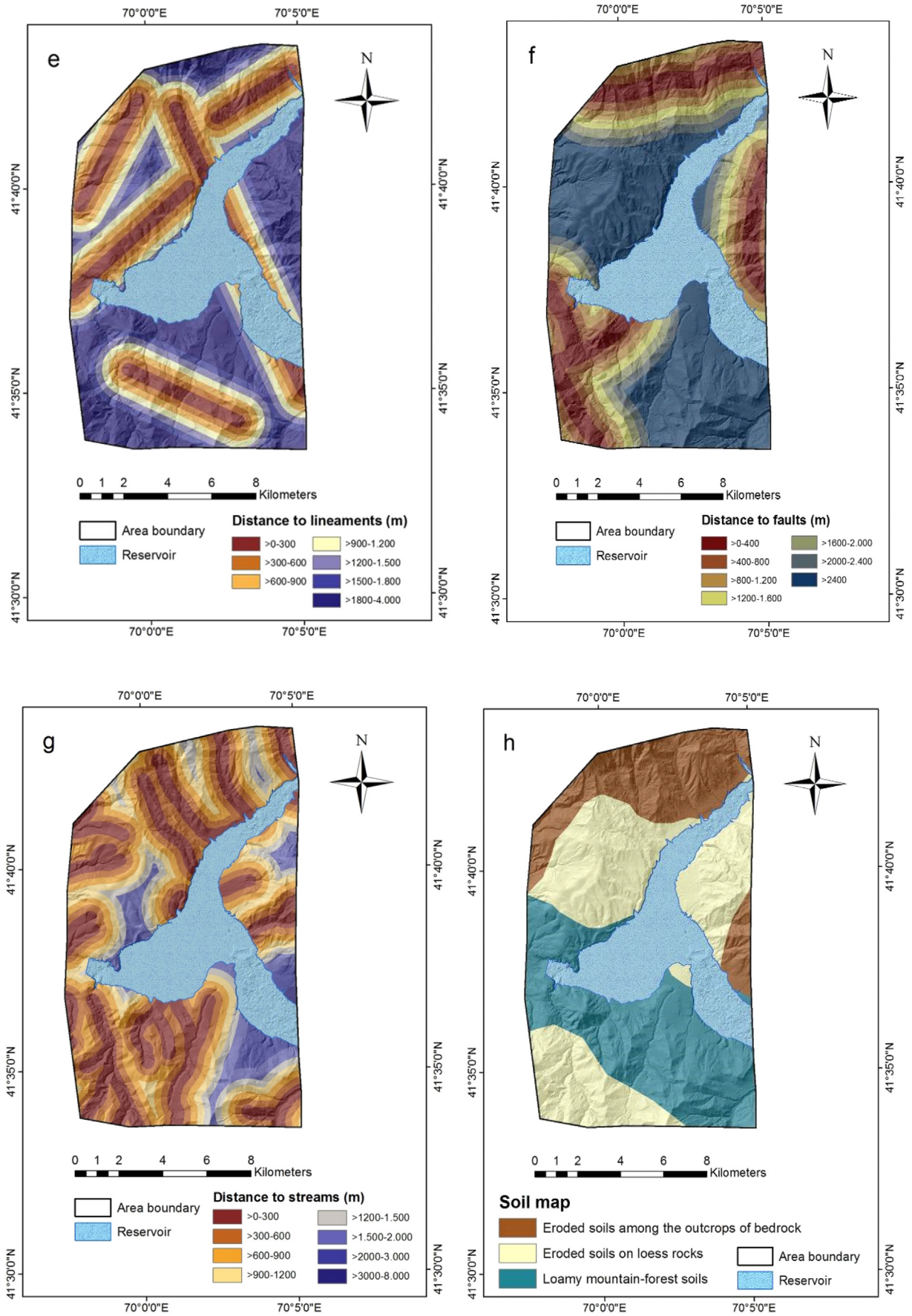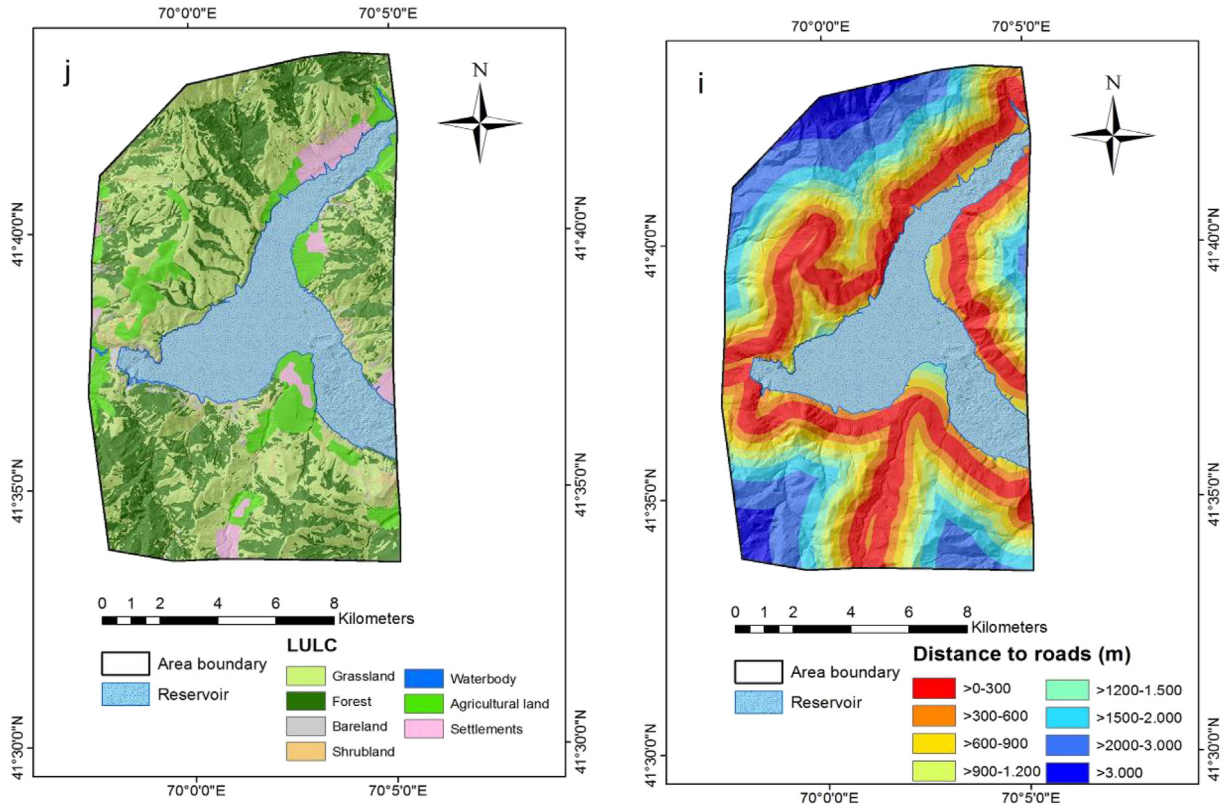
Fig. 2 (*continued*).

Fig. 2 (continued).

of 400 m each (Fig. 2f). Further, bank erosion along water courses plays an important role as a trigger of landslide processes (Park et al., 2013). 44 streams with different lengths are mapped in the study area. The distance to streams layer is classified into eight categories with intervals of 300 m each (Fig. 2g).

2.2.2.3. Soil map. The soil cover on the steep slopes strongly influences landslide occurrence (Sarkar and Kanungo, 2004; Shahabi and Hashim, 2015). The soil map differentiates between three different types of soil including eroded soils associated with outcrops of bedrock, loamy mountain-forest soils and eroded soils on loess rocks (Fig. 2h).

2.2.2.4. Distance to roads. Previous studies suggest that the distance to roads would be an important anthropogenic factor influencing landslide occurrence (Nourani et al., 2014). The roads are digitized from the topographic map, and the distance to the next road is derived for each raster cell. The distance layer is then divided into eight classes with intervals of 300 m each (Fig. 2i).

2.2.2.5. Land use and land cover. According to Constantin et al. (2011) and Pourghasemi et al. (2018) land use and land cover (LULC) is the most commonly used predictor layer after slope, lithology and aspect. Indeed, LULC is a very important parameter with regard to slope stability, even though it has to be considered with care as it may introduce a bias to the results (Steger et al., 2017). The land use and land cover map is classified into seven categories: grassland, forest, bareland, shrubland, water body, agricultural land and settlements (Fig. 2j).

2.3. Methods

Various statistical approaches are available for landslide susceptibility mapping. Three of these methods are employed and compared

within the present study: statistical index (SI), certainty factor (CF) and frequency ratio (FR). The accuracy assessment of the model results is done using the areas under the success rate and prediction rate curves (AUC).

The SI method is a bivariate statistical model proposed by Van Westen et al. (1997). The calculation is based on the correlation of the landslide inventory and the predictor layers. The value of each class is defined as the natural logarithm of the landslide density in the class divided by the landslide density of the study area:

$$W_{ij} = \ln\left(\frac{D_{ij}}{D}\right) = \ln\left[\left(\frac{N_{ij}}{S_{ij}} \middle/ \frac{N}{S}\right)\right]$$

where W_{ij} is the weight given to a certain parameter class (e.g. a rock type or a slope class), D_{ij} is the landslide density within the parameter class, D is the landslide density within the entire map, N_{ij} is the landslide area in a certain parameter class, S_{ij} is the total area in a certain parameter class, N is the total number of the landslide pixels in the study area, and S is the total number of pixels of the study area.

Also the CF method is widely used for landslide susceptibility mapping (Lan et al., 2004):

$$CF = \begin{cases} \dfrac{PP_a - PP_s}{PP_a(1-PP_s)} & \text{if } PP_a \geq PP_s \\ \dfrac{PP_a - PP_s}{PP_s(1-PP_a)} & \text{if } PP_a < PP_s \end{cases}$$

where PP_a is the conditional probability of the landslide event in class a and PP_s is the prior probability of the total number of landslide events occurring in the area. The CF value may vary from −1 to 1. Those values closer to 1 indicate a high certainty of landslide occurrence whereas

Table 3
Spatial relation between thematic layers and landslides using SI, CF and FR methods.

Factor	Class	Class pixels	Slide pixels	Class pixels %	Slide pixels %	SI	CF	FR
LULC	Grassland	623,538	2999	43.59	48.22	0.10	0.09	1.11
	Forest	517,177	2664	36.15	42.83	0.17	0.15	1.18
	Bareland	36,389	265	2.54	4.26	0.51	0.40	1.67
	Shrubland	31,238	284	2.18	4.57	0.73	0.52	2.09
	Waterbody	5710	0	0.40	0.00	0.00	−1.00	0.00
	Agricultural land	160,702	8	11.23	0.13	−4.47	−0.99	0.01
	Settlements	55,713	0	3.89	0.00	0.00	−1.00	0.00
Geology	C1–2	84,203	71	5.88	1.14	−1.64	−0.81	0.19
	Q III–IV	1,347,230	6149	94.12	98.86	0.05	0.04	1.05
Soil	1	343,231	889	23.97	14.29	−0.52	−0.41	0.60
	2	588,508	3516	41.10	56.53	0.31	0.27	1.38
	3	500,223	1815	34.93	29.18	−0.18	−0.17	0.84
Elevation	738–800	7074	0	0.50	0.00	0.00	−1.00	0.00
	800–1000	293,985	998	20.60	16.03	−0.25	−0.22	0.78
	1000–1200	503,422	1783	35.28	28.65	−0.21	−0.19	0.81
	1200–1400	446,522	2843	31.29	45.68	0.38	0.31	1.46
	1400–1600	160,163	583	11.22	9.37	−0.18	−0.16	0.83
	1600–1829	15,697	17	1.10	0.27	−1.39	−0.75	0.25
Aspect	Flat	164,855	642	11.55	10.32	−0.11	−0.11	0.89
	North	168,448	659	11.81	10.59	−0.11	−0.11	0.90
	Northeast	94,694	654	6.64	10.51	0.46	0.37	1.58
	East	257,271	1795	18.03	28.86	0.47	0.37	1.60
	Southeast	76,230	792	5.34	12.73	0.87	0.58	2.38
	South	199,563	418	13.99	6.72	−0.73	−0.52	0.48
	Southwest	85,513	201	5.99	3.23	−0.62	−0.46	0.54
	West	252,155	226	17.67	3.63	−1.58	−0.79	0.21
	Northwest	85,548	672	6.00	10.80	0.59	0.44	1.80
	Northeast	42,586	161	2.98	2.59	−0.14	−0.13	0.87
Slope	1	325,607	496	22.81	7.97	−1.05	−0.65	0.35
	2	647,830	2106	45.38	33.86	−0.29	−0.25	0.75
	3	418,143	3149	29.29	50.63	0.55	0.42	1.73
	4	32,852	441	2.30	7.09	1.12	0.67	3.08
	5	3090	28	0.22	0.45	0.73	0.52	2.08
Distance to lineaments	300	176,158	820	12.31	13.18	0.06	0.06	1.07
	600	195,500	1515	13.66	24.36	0.57	0.44	1.78
	900	209,595	1131	14.65	18.18	0.21	0.19	1.24
	1200	201,533	1208	14.08	19.42	0.32	0.27	1.38
	1500	176,430	103	12.33	1.66	−2.01	−0.87	0.13
	1800	137,282	127	9.59	2.04	−1.55	−0.79	0.21
Distance to faults	400	200,619	413	12.31	13.18	−0.75	−0.53	1.07
	800	176,496	574	13.66	24.36	−0.29	−0.25	1.78
	1200	144,867	985	14.65	18.18	0.44	0.36	1.24
	1600	109,299	453	14.08	19.42	−0.05	−0.05	1.38
	2000	98,704	745	12.33	1.66	0.55	0.42	0.13
	2400	96,885	430	9.59	2.04	0.02	0.02	0.21
	9000	604,420	2620	23.38	21.16	−0.01	−0.01	0.91
Distance to streams	300	377,667	930	26.39	14.95	−0.57	−0.43	0.57
	600	341,322	1081	23.85	17.38	−0.32	−0.27	0.73
	900	257,924	2016	18.02	32.41	0.58	0.44	1.80
	1200	195,378	1194	13.65	19.20	0.34	0.28	1.41
	1500	121,960	199	8.52	3.20	−0.98	−0.62	0.38
	2000	93,981	621	6.57	9.98	0.42	0.34	1.52
	3000	39,736	179	2.78	2.88	0.03	0.03	1.04
	8000	3322	0	0.23	0.00	0.00	−1.00	0.00
Distance to roads	300	338,747	212	23.67	3.41	−1.94	−0.86	0.14
	600	255,531	525	17.85	8.44	−0.75	−0.53	0.47
	900	187,003	655	13.07	10.53	−0.22	−0.20	0.81
	1200	140,898	2208	9.84	35.50	1.28	0.72	3.61
	1500	114,732	705	8.02	11.33	0.34	0.29	1.41
	2000	152,052	1318	10.62	21.19	0.69	0.49	1.99
	3000	175,082	597	12.23	9.60	−0.25	−0.22	0.78
	9000	67,245	0	4.70	0.00	0.00	−1.00	0.00

those values closer to −1 show a low certainty of landslide occurrence. The CF values are incorporated pair wise by using the following combination rule:

$$Z = \begin{cases} CF1 + CF2 - CF1 CF2 & CF1, CF2 \geq 0 \\ CF1 + CF2 + CF1 CF2 & CF1, CF2 < 0 \\ \dfrac{CF1 + CF2}{1 - min(|CF1|, |CF2|)} & CF1 * CF2 < 0 \end{cases}$$

According to Pourghasemi et al. (2018), the FR method is the most utilized approach for landslide susceptibility mapping after logistic regression. As a bivariate statistical method, the FR approach shows the correlation between the landslides and each single predictor layer (Lee and Pradhan, 2007). The landslide susceptibility index is derived by summarizing all layer-specific factor values:
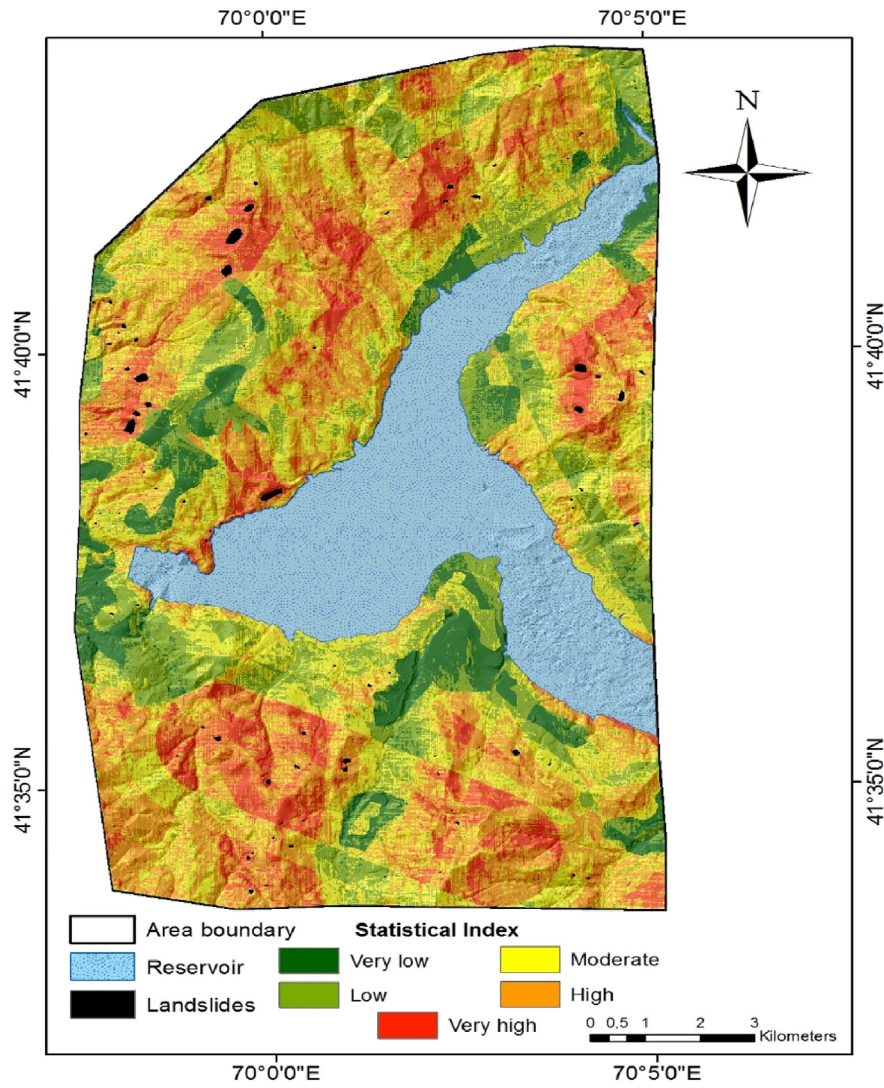
$$LSI = \sum FR$$

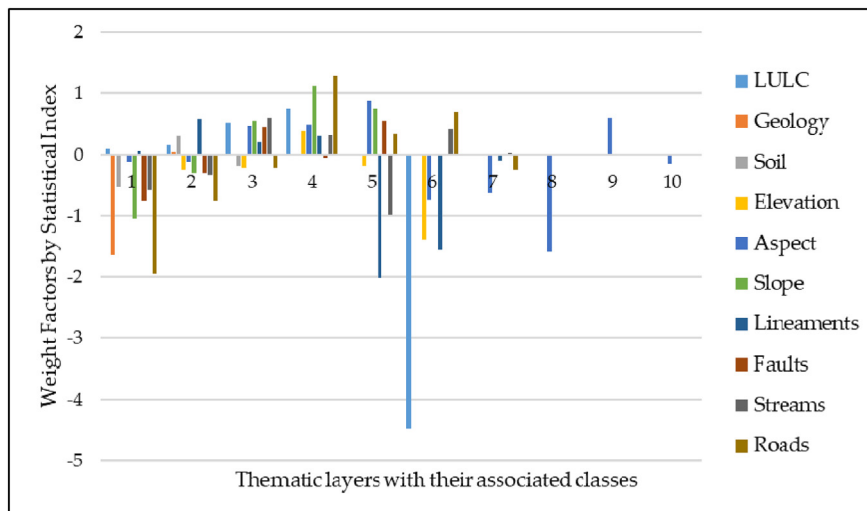**Fig. 3.** Landslide susceptibility map derived using the statistical index (SI) method.

Fig. 4. Weight factors of predictor layers for the statistical index (SI) method.

3. Results

3.1. Landslide susceptibility mapping using the SI method

The spatial relationships between the predictor layers and the landslide inventory for the SI method are shown in Table 3. The final susceptibility map is divided into five classes based on the natural breaks method: very low, low, moderate, high, and very high (Fig. 3). The weights associated to each class of each predictor layer vary over a broad range (Fig. 4). Among the LULC predictor layer classes, bareland and shrubland have the highest weight factors of 0.51 and 0.73 respectively, indicating that these two classes are most susceptible to landslide occurrence. The alluvial complex covered by loess deposits shows the highest weight factor (0.05) among the geological units. Among the soil classes, loamy mountain-forest soils show the highest susceptibility (weight factor of 0.31), whereas the lowest value is derived for eroded soils associated with outcrops of bedrock (−0.52). Also the DEM-derived layers play an important role for landslide susceptibility, whereby the elevation class from 1200 to 1400 m shows the highest weight factor (0.38) and the lowest value is derived for the elevation class above 1600 m. East, northwest and southeast facing slopes are most susceptible among the aspect classes (0.47, 0.59 and 0.87, respectively). The weight factor for the slope increases from 20°–35°onwards and reaches its maximum value of 1.12 in the class 35°–45°. Considering the distance to lineaments layer, the range between 300 and 600 m has the highest weight factor (0.57), whereas the most susceptible class of the distance to faults layer corresponds to the range 800–1200 m (0.44). The highest SI value for the distance to streams layer is computed for the class 600–900 m. The most susceptible class from the distance to roads layer belongs to the range between 900 and 1200 m. The percentage of the classes very low, low, moderate, high and very high of the susceptibility map computed with the statistical index method are 11.64, 20.41, 24.58, 35.61 and 7.76%, respectively (Fig. 5).

3.2. Landslide susceptibility mapping using the CF method

The spatial relationships between the predictor layers and the landslide inventory for the CF method are shown in Table 3. The final susceptibility map derived with the CF method was divided into five classes using natural breaks (Fig. 6). The LULC layer has the highest values for the classes bareland and shrubland (0.40, 0.52 respectively), indicating that these two classes are most susceptible to landslide occurrence. The alluvial complex covered by loess deposits shows the highest weight factor (0.04) among the geological units. Among the soil units, loamy

mountain-forest soils have a value of 0.27: they represent the most susceptible class derived from the soil map layer. The elevation class from 1200 to 1400 m shows the highest weight factor (0.31), whereas the lowest value is derived for the elevation class up to 800 m (Fig. 7). The northeast, east, southeast and northwest facing slopes show values of 0.37, 0.37, 0.58 and 0.44 respectively. For the slope layer the susceptibility increases from 20° to 65°. The class 300–600 m shows the highest degree of susceptibility (0.44) with regard to the distance to lineaments. The class from 800 to 1200 m is most susceptible with regard to the distance to faults, the class from 600 to 900 m with regard to the distance to streams, and the class from 900 to 1200 m with regard to the distance to roads. The percentage of the classes showing very low, low, moderate, high and very high landslide susceptibility are 11.04, 25.95, 26.67, 30.10, and 6.25%, respectively (Fig. 5).

3.3. Landslide susceptibility mapping using the FR method

The spatial relationships between the predictor layers and the landslide inventory for the FR method are shown in Table 3. For the FR method values <1 show a low susceptibility and >1 a high susceptibility to landslides. The final susceptibility map derived with the FR method is divided into five classes using natural breaks (Fig. 8). Among the LULC predictor layer grassland, shrubland and bareland are most susceptible to landslide occurrence, with values of 1.11, 2.09 and 1.67, respectively. The lowest values are associated to the classes of water bodies and settlements. Among the geological units the alluvial complex has a weight of 1.05 and it is the most susceptible class. Among the soil classes the loamy mountain-forest soils have the highest susceptibility value (1.38), the lowest value falls on eroded soils among the outcrops of bedrock (0.60) (Fig. 9). Considering the elevation classes, the range between 1200 and 1400 m shows the highest susceptibility (1.46). The northeast, east, southeast, and northwest facing slopes are most susceptible with regard to slope aspect (1.58, 1.60, 2.38, and 1.80 respectively). The weight factor for the slope increases from 20°–35° to 35°–45° (values of 1.73 and 3.08, respectively) and decreases for the class 45°–62° (2.08). Considering the distance to lineaments layer, the first four classes have values above 1. Also the first four classes of the distance to faults layer show the highest susceptibilities to landslide occurrence, and so do the ranges between 600 and 1200 m of the distance to streams layer (values of 1.80 and 1.41, respectively). For the layer distance to roads, the highest values are displayed for the classes 900–1200 m, 1200–1500 m, and 1500–2000 m, with values of 3.61, 1.41, and 1.99, respectively. The percentages of the classes very low, low, moderate, high, and very high throughout the entire landslide
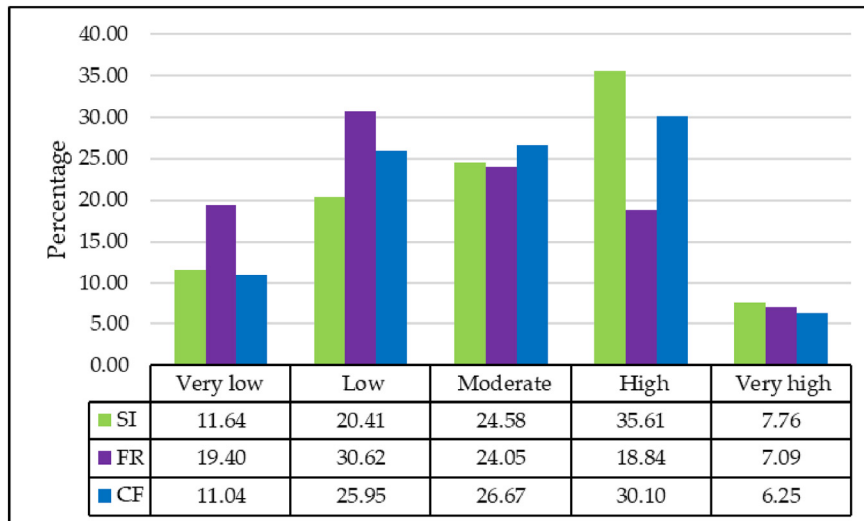

	Very low	Low	Moderate	High	Very high
■ SI	11.64	20.41	24.58	35.61	7.76
■ FR	19.40	30.62	24.05	18.84	7.09
■ CF	11.04	25.95	26.67	30.10	6.25

Fig. 5. The percentage of the different susceptibility classes for the statistical index (SI), frequency ratio (FR) and certainty factor (CF) methods.
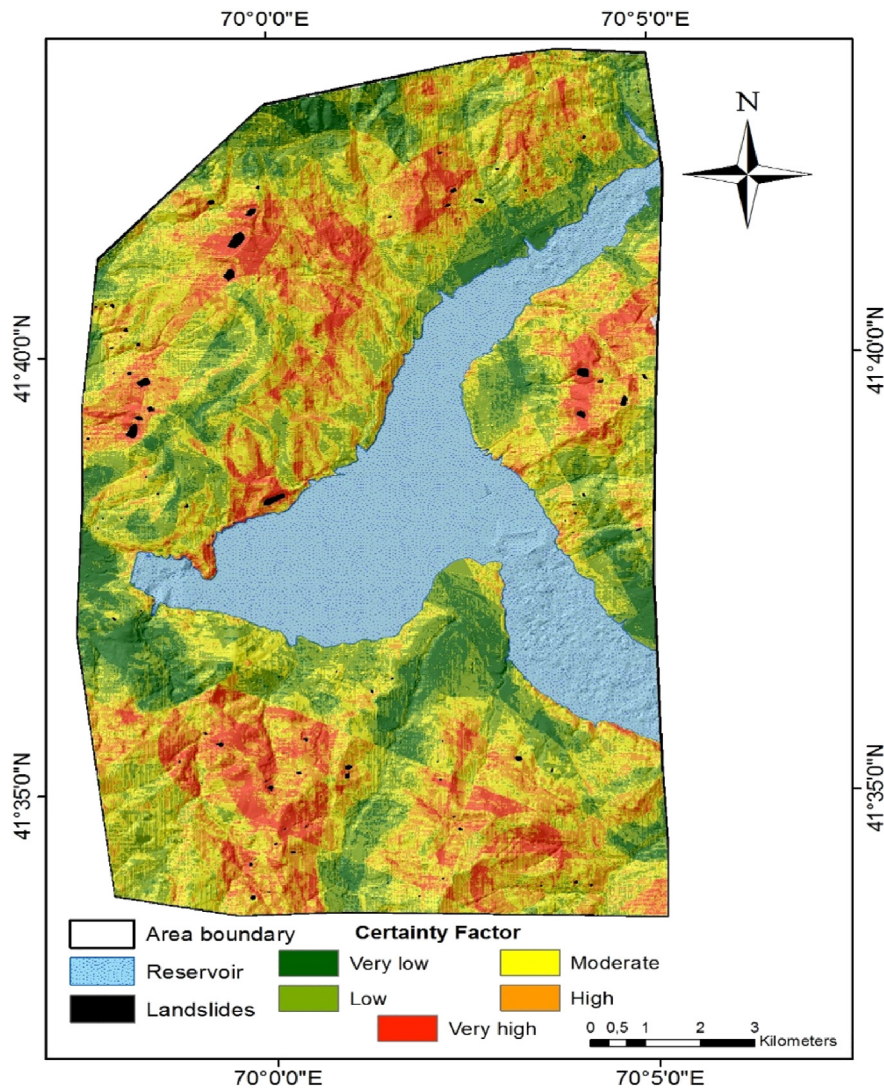
Fig. 6. Landslide susceptibility map derived using the certainty factor (CF) method.

susceptibility map are 19.40, 30.62, 24.05, 18.84, and 7.09%, respectively (Fig. 5).

3.4. Evaluation against the landslide inventory

The success rates of the SI, FR and CF methods are shown in Fig. 10. The AUC value for the SI method is 0.821, corresponding to a training accuracy of 82.1%. The AUC value for the CF method is 0.743, corresponding to a training accuracy of 74.3%. For the FR method an AUC value of 0.74, corresponding to a training accuracy of 74%, is obtained. The prediction rates associated to the SI, CF and FR methods are summarized in Fig. 11: the AUC value obtained with the SI method is 0.8 and the prediction accuracy is, consequently, 80%. The AUC value for the CF method is 0.7 and the prediction accuracy is 70%. For the FR method the AUC value is 0.71 and the prediction accuracy is 71%. These evaluation results reveal that the FR and CF methods perform in a similar way for our study area, whereas the SI method yields the best result in terms of empirical adequacy.

4. Discussion

Landslide susceptibility mapping is important for visualizing potentially landslide-prone areas in hilly and mountainous terrain (Dou et al., 2015a, 2015b). Several authors have performed statistical landslide susceptibility analyses for various areas worldwide. Wu et al. (2016), for example, applied the SI, FR, and CF methods for a landslide susceptibility assessment for the Gangu County, China. They used 12 predictor layers and a point-based landslide inventory with a cell size of 30x30m. The AUC method was used for the evaluation of the models, yielding accuracies of the three methods around 75%. Zhao et al. (2015) applied the SI and CF methods to analyze landslide susceptibility in the Shangzhou district, Shaanxi province, China. They mapped 145 landslide locations as points using a cell size of 50x50m. The AUC method revealed accuracies of the applied methods between 68 and 70%.

Preliminary knowledge about the predictor layers conditioning the spatial patterns of landslide occurrence is desired (Guzzetti et al., 1999). Landslide susceptibility analyses require several types of input data. The selection of the appropriate predictor layers depends on a variety of factors such as study area scale and pattern, type of landslide processes, and data availability and quality (Manzo et al., 2013; Tien Bui et al., 2016). Hence, the number of predictor layers can vary, depending on the study area. According to Pourghasemi et al. (2018), the predictor layers selected for the current study are in general the most used layers for landslide susceptibility analysis. Some of the landslide-predictor relationships are now discussed in more detail: all three methods applied reveal that the bareland and shrubland classes from the LULC layer are most susceptible to landslides. So is loose
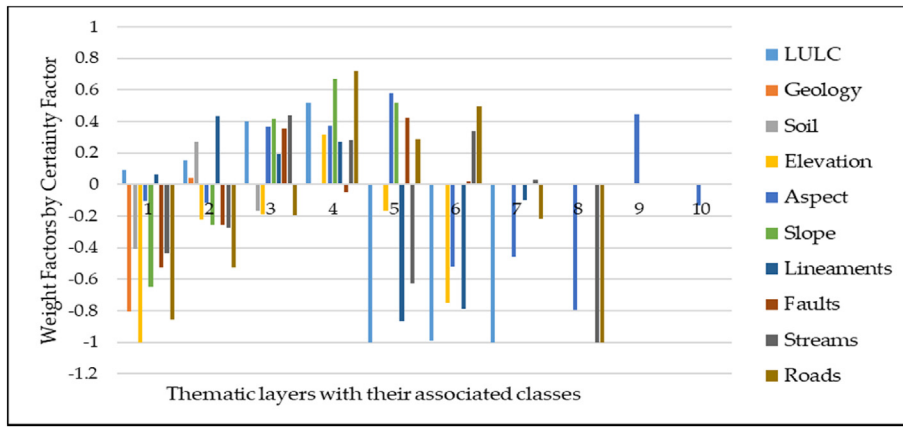
Fig. 7. Weight factors of predictor layers for the certainty factor method.

material from the quaternary alluvial complex. Further, a decrease of landslide susceptibility with elevation is observed (Zare et al., 2013). This can be explained by the fact that hard bedrock often prevails at high elevation (Mohammady et al., 2012). For our study area the elevation range between 1200 and 1400 m displays the highest landslide susceptibility for all three methods, whereas the susceptibility decreases above this range. Due to increasing shear stress with increasing slope, slopes between 35° and 45° show the highest susceptibility for all three methods. Steeper slopes mostly occur in bedrock. Among the slope aspect layer classes, the highest susceptibility values are associated to southeast facing slopes due to the general orientation of the geological layers. The patterns of landslide susceptibility with regard to
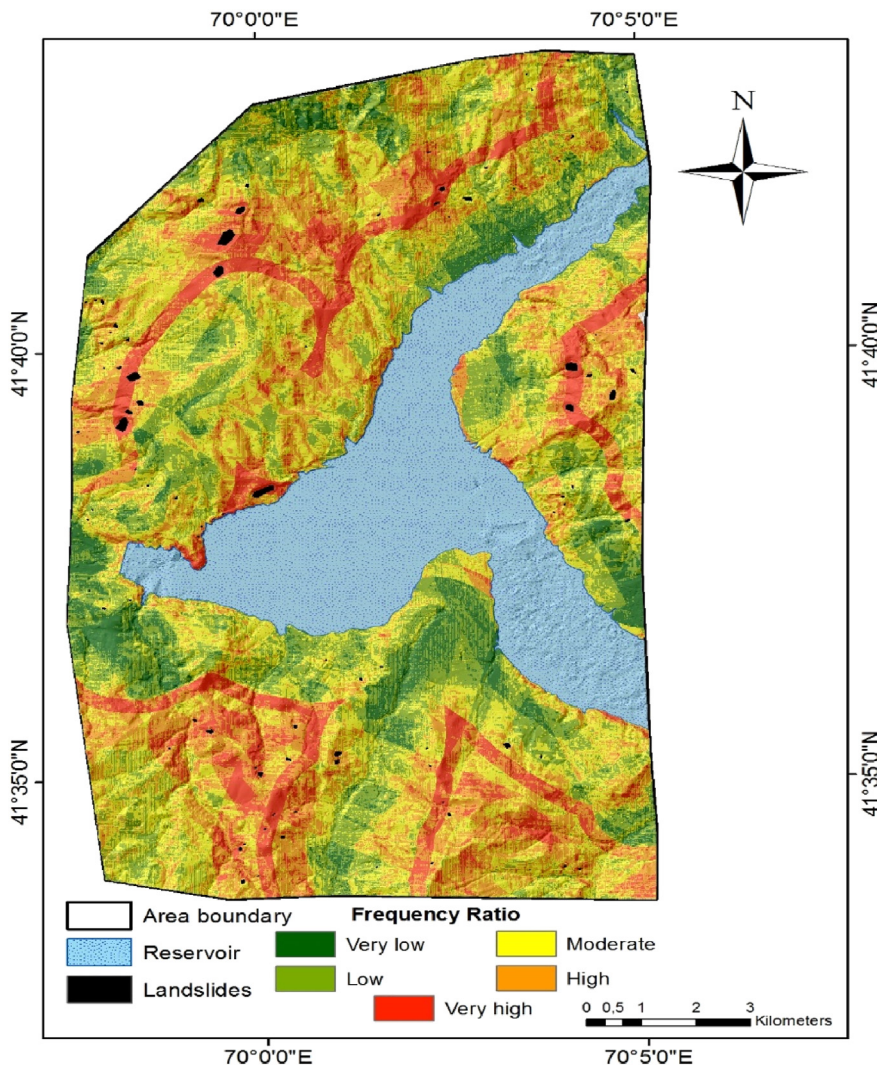

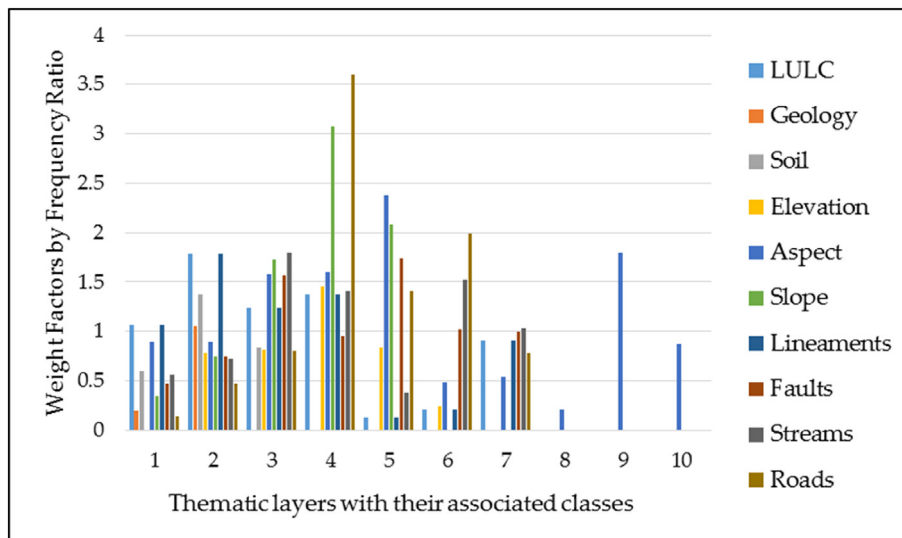Fig. 8. Landslide susceptibility map derived using the frequency ratio (FR) method.

Fig. 9. Weight factors of predictor layers for the frequency ratio method.

each predictor layer are largely similar for all three methods employed, and many findings of earlier studies could be confirmed, indicating a certain robustness of the results.

Also the derived AUC results are promising. The maximum accuracy (82%) was achieved with the SI method. It is higher than the accuracies yielded in many other studies (Regmi et al., 2014; Dou et al., 2015a, 2015b; Zhao et al., 2015; Cui et al., 2017; Vakhshoori and Zare, 2016; Hong et al., 2016) which commonly arrived at accuracies between 70% and 80%. We may assume that this higher accuracy is a result of using a polygon-based instead of a point-based inventory, as it was done in most earlier studies. However, more research is necessary to confirm this hypothesis. In general, the benefit of using polygon-based landslide inventories depends on landslide size and geometry (Zêzere et al., 2017).

The at least 18% of the observed landslide distribution not explained by the models are most probably the result of a combination of (i) uncertainties in the spatial patterns of the predictor layers; (ii) influence of additional factors not considered in the present work; (iii) positional errors (Steger et al., 2016) or incompleteness (Steger et al., 2017) of the mapped landslides; and (iv) mistakes in the interpretation of the satellite images.

The study area is seismically active and the precipitation is higher than it is reported for adjacent regions. However, there are no high-resolution precipitation and seismic data available for the 177 km^2 large study area. Extending the landslide susceptibility mapping to larger areas could profit from the availability of precipitation and seismic data, as these layers can be crucial for the spatial patterns of landslide susceptibility, and their inclusion may therefore improve the quality of the results.

5. Conclusions

The active seismicity and the high amount of precipitation make the Bostanlik district highly susceptible to landslide processes. The selection of methods and predictor layers used for the landslide susceptibility mapping conducted in the present study builds on the available data and on the study area size. The three statistical methods statistical index (SI), frequency ratio (FR) and certainty factor (CF) were selected for the landslide susceptibility mapping, relating a set of ten predictor layers to a landslide inventory. The three landslide susceptibility maps were split into five classes, i.e. very low, low, moderate, high, very high, based on natural breaks. The model performance was analyzed
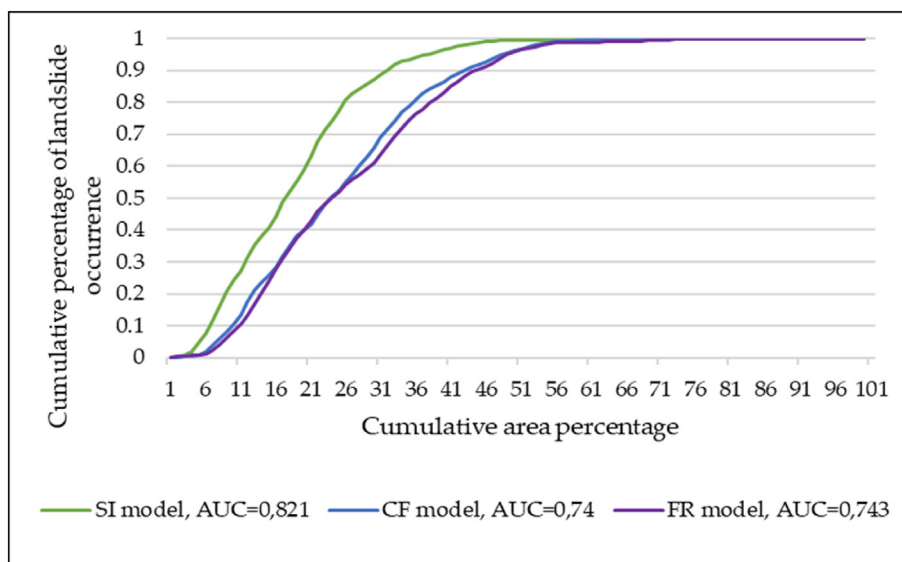

Fig. 10. Success rate curves of the landslide susceptibility maps for the statistical index (SI), frequency ratio (FR) and certainty factor (CF) methods.
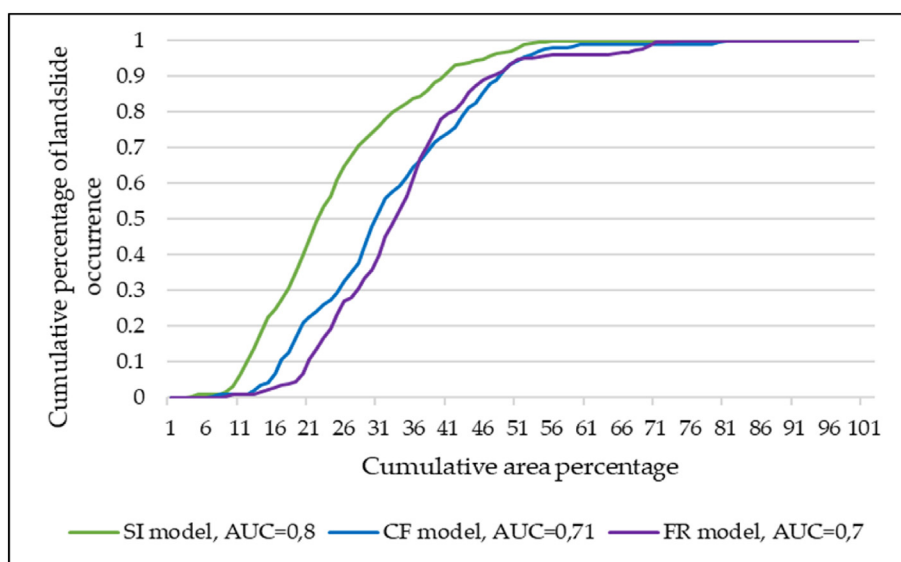
Fig. 11. Prediction rate curves of the landslide susceptibility maps for the statistical index (SI), frequency ratio (FR) and certainty factor (CF) methods.

using the area under curve (AUC). The AUC plots showed that the training accuracies were 82.1%, 74.3% and 74%, whereas the prediction accuracies were 80%, 70% and 71%, for the SI, FR and CF methods, respectively. The FR and CF methods performed in a similar way whereas the SI method yielded the highest accuracy among all the methods applied. The relationships between the landslide inventory and the predictor layers largely confirmed the results of previous studies. Model performance was slightly higher than in some previous studies using the same methods for other areas, which is possibly a result of using a polygon-based landslide inventory derived from high-resolution satellite imagery. Further research is necessary to clarify the influence of the type of landslide inventory on the performance of statistical landslide susceptibility analyses. In the future, landslide susceptibility mapping will be extended to larger areas with the cooperation of local, regional and national authorities, who need the results for prioritizing areas requiring further attention.

Acknowledgements

References

Akbari, A., Yahaya, F.B.M., Azamirad, M., Fanodi, M., 2014. Landslide susceptibility mapping using logistic regression analysis and GIS tools. Electron. J. Geotech. Eng. 19, 1687–1696.

Akgun, A., 2012. A comparison of landslide susceptibility maps produced by logistic regression, multi-criteria decision, and likelihood ratio methods: a case study at İzmir, Turkey. Landslides 9, 93–106. https://doi.org/10.1007/s10346-011-0283-7.

Althuwaynee, O.F., Pradhan, B., Lee, S., 2012. Application of an evidential belief function model in landslide susceptibility mapping. Comput. Geosci. 44, 120–135. https://doi.org/10.1016/j.cageo.2012.03.003.

Basharat, M., Shah, H.R., Hameed, N., 2016. Landslide susceptibility mapping using GIS and weighted overlay method: a case study from NW Himalayas, Pakistan. Arab. J. Geosci. 9. https://doi.org/10.1007/s12517-016-2308-y.

Belolipov, I.V., Zaurov, D.E., Eisenman, S.W., 2013. The geography, climate and vegetation of Uzbekistan. In: Eisenman, S.W., Zaurov, D.E., Struwe, L. (Eds.), Medicinal Plants of Central Asia: Uzbekistan and Kyrgyzstan. Springer New York, New York, NY, pp. 5–7 (ISBN 978-1-4614-3911-0).

Bilaşco, Ş., Horvath, C., Roşian, G., Sorin, F., Keller, I.E., 2011. Statistical model using GIS for the assessment of landslide susceptibility. Case-study: the Someş plateau. Romanian J. Geogr. Ed. Acad. Rom. Bucur.

Catani, F., Lagomarsino, D., Segoni, S., Tofani, V., 2013. Landslide susceptibility estimation by random forests technique: sensitivity and scaling issues. Nat. Hazards Earth Syst. Sci. 13, 2815–2831. https://doi.org/10.5194/nhess-13-2815-2013.

Central Asia and Caucasus Disaster Risk Management Initiative (CAC DRMI), 2009. Risk Assessment for Central Asia and Caucasus Desk Study Review.

Chen, W., Chai, H., Sun, X., Wang, Q., Ding, X., Hong, H., 2016. A GIS-based comparative study of frequency ratio, statistical index and weights-of-evidence models in landslide susceptibility mapping. Arab. J. Geosci. 9. https://doi.org/10.1007/s12517-015-2150-7.

Chen, W., Peng, J., Hong, H., Shahabi, H., Pradhan, B., Liu, J., Zhu, A.-X., Pei, X., Duan, Z., 2018. Landslide susceptibility modelling using GIS-based machine learning techniques for Chongren County, Jiangxi Province, China. Sci. Total Environ. 626, 1121–1135. https://doi.org/10.1016/j.scitotenv.2018.01.124.

Constantin, M., Bednarik, M., Jurchescu, M.C., Vlaicu, M., 2011. Landslide susceptibility assessment using the bivariate statistical analysis and the index of entropy in the Sibiciu Basin (Romania). Environ. Earth Sci. 63, 397–406. https://doi.org/10.1007/s12665-010-0724-y.

Cui, K., Lu, D., Li, W., 2017. Comparison of landslide susceptibility mapping based on statistical index, certainty factors, weights of evidence and evidential belief function models. Geocarto Int. 32, 935–955. https://doi.org/10.1080/10106049.2016.1195886.

Devkota, K.C., Regmi, A.D., Pourghasemi, H.R., Yoshida, K., Pradhan, B., Ryu, I.C., Dhital, M.R., Althuwaynee, O.F., 2013. Landslide susceptibility mapping using certainty factor, index of entropy and logistic regression models in GIS and their comparison at Mugling–Narayanghat road section in Nepal Himalaya. Nat. Hazards 65, 135–165. https://doi.org/10.1007/s11069-012-0347-6.

Dou, J., Chang, K.-T., Chen, S., Yunus, A., Liu, J.-K., Xia, H., Zhu, Z., 2015a. Automatic case-based reasoning approach for landslide detection: integration of object-oriented image analysis and a genetic algorithm. Remote Sens. 7, 4318–4342. https://doi.org/10.3390/rs70404318.

Dou, J., Tien Bui, D., Yunus, A., Jia, K., Song, X., Revhaug, I., Xia, H., Zhu, Z., 2015b. Optimization of causative factors for landslide susceptibility evaluation using remote sensing and GIS data in parts of Niigata, Japan. PLoS ONE 10, e0133262. https://doi.org/10.1371/journal.pone.0133262.

Ercanoglu, M., Gokceoglu, C., Van Asch, T.W., 2004. Landslide susceptibility zoning north of Yenice (NW Turkey) by multivariate statistical techniques. Nat. Hazards 32, 1–23.

Fan, W., Wei, X., Cao, Y., Zheng, B., 2017. Landslide susceptibility assessment using the certainty factor and analytic hierarchy process. J. Mt. Sci. 14, 906–925. https://doi.org/10.1007/s11629-016-4068-2.

Golovko, D., Roessner, S., Behling, R., Wetzel, H.-U., Kleinschmit, B., 2017. Evaluation of remote-sensing-based landslide inventories for hazard assessment in Southern Kyrgyzstan. Remote Sens. 9, 943. https://doi.org/10.3390/rs9090943.

Gutiérrez, F., Linares, R., Roqué, C., Zarroca, M., Carbonel, D., Rosell, J., Gutiérrez, M., 2015. Large landslides associated with a diapiric fold in Canelles Reservoir (Spanish Pyrenees): detailed geological–geomorphological mapping, trenching and electrical resistivity imaging. Geomorphology 241, 224–242. https://doi.org/10.1016/j.geomorph.2015.04.016.

Guzzetti, F., Carrara, A., Cardinali, M., Reichenbach, P., 1999. Landslide hazard evaluation: a review of current techniques and their application in a multi-scale study, Central Italy. Geomorphology 31, 181–216. https://doi.org/10.1016/S0169-555X(99)00078-1.

Guzzetti, F., Reichenbach, P., Ardizzone, F., Cardinali, M., Galli, M., 2006. Estimating the quality of landslide susceptibility models. Geomorphology 81, 166–184. https://doi.org/10.1016/j.geomorph.2006.04.007.

Hong, H., Chen, W., Xu, C., Youssef, A.M., Pradhan, B., Tien Bui, D., 2016. Rainfall-induced landslide susceptibility assessment at the Chongren area (China) using frequency ratio, certainty factor, and index of entropy. Geocarto Int., 1–16 https://doi.org/10.1080/10106049.2015.1130086.

Hong, H., Liu, J., Zhu, A.-X., Shahabi, H., Pham, B.T., Chen, W., Pradhan, B., Bui, D.T., 2017. A novel hybrid integration model using support vector machines and random subspace for weather-triggered landslide susceptibility assessment in the Wuning area (China). Environ. Earth Sci. 76. https://doi.org/10.1007/s12665-017-6981-2.

Hong, H., Liu, J., Bui, D.T., Pradhan, B., Acharya, T.D., Pham, B.T., Zhu, A.-X., Chen, W., Ahmad, B.B., 2018. Landslide susceptibility mapping using J48 Decision Tree with AdaBoost, Bagging and Rotation Forest ensembles in the Guangchang area (China). Catena 163, 399–413. https://doi.org/10.1016/j.catena.2018.01.005.

Hussin, H.Y., Zumpano, V., Reichenbach, P., Sterlacchini, S., Micu, M., van Westen, C., Bălteanu, D., 2016. Different landslide sampling strategies in a grid-based bi-variate statistical susceptibility model. Geomorphology 253, 508–523. https://doi.org/10.1016/j.geomorph.2015.10.030.

Ilia, I., Tsangaratos, P., 2016. Applying weight of evidence method and sensitivity analysis to produce a landslide susceptibility map. Landslides 13, 379–397. https://doi.org/10.1007/s10346-015-0576-3.

Juliev, M., Pulatov, A., Hubl, J., 2017. Natural hazards in mountain regions of Uzbekistan: a review of mass movement processes in Tashkent province. Int. J. Sci. Eng. Res. 8, 1102–1108. https://doi.org/10.14299/ijser.2017.02.013.

Lan, H.X., Zhou, C.H., Wang, L.J., Zhang, H.Y., Li, R.H., 2004. Landslide hazard spatial analysis and prediction using GIS in the Xiaojiang watershed, Yunnan, China. Eng. Geol. 76, 109–128. https://doi.org/10.1016/j.enggeo.2004.06.009.

Lee, S., Pradhan, B., 2007. Landslide hazard mapping at Selangor, Malaysia using frequency ratio and logistic regression models. Landslides 4, 33–41. https://doi.org/10.1007/s10346-006-0047-y.

Manzo, G., Tofani, V., Segoni, S., Battistini, A., Catani, F., 2013. GIS techniques for regional-scale landslide susceptibility assessment: the Sicily (Italy) case study. Int. J. Geogr. Inf. Sci. 27, 1433–1452. https://doi.org/10.1080/13658816.2012.693614.

Meinhardt, M., Fink, M., Tünschel, H., 2015. Landslide susceptibility analysis in central Vietnam based on an incomplete landslide inventory: comparison of a new method to calculate weighting factors by means of bivariate statistics. Geomorphology 234, 80–97. https://doi.org/10.1016/j.geomorph.2014.12.042.

Meten, M., PrakashBhandary, N., Yatabe, R., 2015. Effect of landslide factor combinations on the prediction accuracy of landslide susceptibility maps in the Blue Nile Gorge of Central Ethiopia. Geoenviron. Disasters 2. https://doi.org/10.1186/s40677-015-0016-7.

Mohammady, M., Pourghasemi, H.R., Pradhan, B., 2012. Landslide susceptibility mapping at Golestan Province, Iran: a comparison between frequency ratio, Dempster–Shafer, and weights-of-evidence models. J. Asian Earth Sci. 61, 221–236. https://doi.org/10.1016/j.jseaes.2012.10.005.

Niyazov, R., Nurtaev, B., 2013. Modern seismogenic landslides caused by the Pamir-Hindu Kush earthquakes and their consequences in central Asia. In: Margottini, C., Canuti, P., Sassa, K. (Eds.), Landslide Science and Practice: Volume 5: Complex Environment. Springer Berlin Heidelberg, Berlin, Heidelberg, pp. 343–348 (ISBN 978-3-642-31427-8).

Nourani, V., Pradhan, B., Ghaffari, H., Sharifi, S.S., 2014. Landslide susceptibility mapping at Zonouz Plain, Iran using genetic programming and comparison with frequency ratio, logistic regression, and artificial neural network models. Nat. Hazards 71, 523–547. https://doi.org/10.1007/s11069-013-0932-3.

Ozdemir, A., Altural, T., 2013. A comparative study of frequency ratio, weights of evidence and logistic regression methods for landslide susceptibility mapping: Sultan Mountains, SW Turkey. J. Asian Earth Sci. 64, 180–197. https://doi.org/10.1016/j.jseaes.2012.12.014.

Park, S., Choi, C., Kim, B., Kim, J., 2013. Landslide susceptibility mapping using frequency ratio, analytic hierarchy process, logistic regression, and artificial neural network methods at the Inje area, Korea. Environ. Earth Sci. 68, 1443–1464. https://doi.org/10.1007/s12665-012-1842-5.

Pourghasemi, H.R., Pradhan, B., Gokceoglu, C., 2012. Application of fuzzy logic and analytical hierarchy process (AHP) to landslide susceptibility mapping at Haraz watershed, Iran. Nat. Hazards 63, 965–996. https://doi.org/10.1007/s11069-012-0217-2.

Pourghasemi, H.R., Pradhan, B., Gokceoglu, C., Mohammadi, M., Moradi, H.R., 2013. Application of weights-of-evidence and certainty factor models and their comparison in landslide susceptibility mapping at Haraz watershed, Iran. Arab. J. Geosci. 6, 2351–2365. https://doi.org/10.1007/s12517-012-0532-7.

Pourghasemi, H.R., Teimoori Yansari, Z., Panagos, P., Pradhan, B., 2018. Analysis and evaluation of landslide susceptibility: a review on articles published during 2005–2016 (periods of 2005–2012 and 2013–2016). Arab. J. Geosci., 11 https://doi.org/10.1007/s12517-018-3531-5.

Regmi, A.D., Devkota, K.C., Yoshida, K., Pradhan, B., Pourghasemi, H.R., Kumamoto, T., Akgun, A., 2014. Application of frequency ratio, statistical index, and weights-of-

evidence models and their comparison in landslide susceptibility mapping in Central Nepal Himalaya. Arab. J. Geosci. 7, 725–742. https://doi.org/10.1007/s12517-012-0807-z.

Saponaro, A., Pilz, M., Bindi, D., Parolai, S., 2015a. The contribution of EMCA to landslide susceptibility mapping in Central Asia. Ann. Geophys. 58.

Saponaro, A., Pilz, M., Wieland, M., Bindi, D., Moldobekov, B., Parolai, S., 2015b. Landslide susceptibility analysis in data-scarce regions: the case of Kyrgyzstan. Bull. Eng. Geol. Environ. 74, 1117–1136. https://doi.org/10.1007/s10064-014-0709-2.

Sara, F., Silvia, B., Sandro, M., 2015. Landslide inventory updating by means of Persistent Scatterer Interferometry (PSI): the Setta basin (Italy) case study. Geomat. Nat. Haz. Risk 6, 419–438. https://doi.org/10.1080/19475705.2013.866985.

Sarkar, S., Kanungo, D.P., 2004. An integrated approach for landslide susceptibility mapping using remote sensing and GIS. Photogramm. Eng. Remote. Sens. 70, 617–625.

Sato, H.P., Harp, E.L., 2009. Interpretation of earthquake-induced landslides triggered by the 12 May 2008, M7.9 Wenchuan earthquake in the Beichuan area, Sichuan Province, China using satellite imagery and Google Earth. Landslides 6, 153–159. https://doi.org/10.1007/s10346-009-0147-6.

Shahabi, H., Hashim, M., 2015. Landslide susceptibility mapping using GIS-based statistical models and remote sensing data in tropical environment. Sci. Rep. 5. https://doi.org/10.1038/srep09899.

Steger, S., Brenning, A., Bell, R., Glade, T., 2016. The propagation of inventory-based positional errors into statistical landslide susceptibility models. Nat. Hazards Earth Syst. Sci. 16 (12), 2729–2745.

Steger, S., Brenning, A., Bell, R., Glade, T., 2017. The influence of systematically incomplete shallow landslide inventories on statistical susceptibility models and suggestions for improvements. Landslides 14, 1767–1781. https://doi.org/10.1007/s10346-017-0820-0.

Teerarungsigul, S., Torizin, J., Fuchs, M., Kühn, F., Chonglakmani, C., 2016. An integrative approach for regional landslide susceptibility assessment using weight of evidence method: a case study of Yom River Basin, Phrae Province, Northern Thailand. Landslides 13, 1151–1165. https://doi.org/10.1007/s10346-015-0659-1.

Tien Bui, D., Pradhan, B., Lofman, O., Revhaug, I., Dick, Ø.B., 2013. Regional prediction of landslide hazard using probability analysis of intense rainfall in the Hoa Binh province, Vietnam. Nat. Hazards 66, 707–730. https://doi.org/10.1007/s11069-012-0510-0.

Tien Bui, D., Tuan, T.A., Klempe, H., Pradhan, B., Revhaug, I., 2016. Spatial prediction models for shallow landslide hazards: a comparative assessment of the efficacy of support vector machines, artificial neural networks, kernel logistic regression, and logistic model tree. Landslides 13, 361–378. https://doi.org/10.1007/s10346-015-0557-6.

Vakhshoori, V., Zare, M., 2016. Landslide susceptibility mapping by comparing weight of evidence, fuzzy logic, and frequency ratio methods. Geomat. Nat. Haz. Risk 7, 1731–1752. https://doi.org/10.1080/19475705.2016.1144655.

Van Westen, C.J., 2002. Use of Weights of Evidence Modeling for Landslide Susceptibility Mapping. Int. Inst. Geoinformation Sci. Earth Obs, Enschede Neth.

Van Westen, C.J., Rengers, N., Terlien, M.T.J., Soeters, R., 1997. Prediction of the occurrence of slope instability phenomenal through GIS-based hazard zonation. Geol. Rundsch. 86, 404–414.

Van Westen, C.J., Castellanos, E., Kuriakose, S.L., 2008. Spatial data for landslide susceptibility, hazard, and vulnerability assessment: an overview. Eng. Geol. 102, 112–131. https://doi.org/10.1016/j.enggeo.2008.03.010.

Wang, Q., Li, W., Chen, W., Bai, H., 2015. GIS-based assessment of landslide susceptibility using certainty factor and index of entropy models for the Qianyang County of Baoji city, China. J. Earth Syst. Sci. 124, 1399–1415.

Wu, Y., Li, W., Wang, Q., Liu, Q., Yang, D., Xing, M., Pei, Y., Yan, S., 2016. Landslide susceptibility assessment using frequency ratio, statistical index and certainty factor models for the Gangu County, China. Arab. J. Geosci. 9. https://doi.org/10.1007/s12517-015-2112-0.

Zare, M., Pourghasemi, H.R., Vafakhah, M., Pradhan, B., 2013. Landslide susceptibility mapping at Vaz Watershed (Iran) using an artificial neural network model: a comparison between multilayer perceptron (MLP) and radial basic function (RBF) algorithms. Arab. J. Geosci. 6, 2873–2888. https://doi.org/10.1007/s12517-012-0610-x.

Zêzere, J.L., Pereira, S., Melo, R., Oliveira, S.C., Garcia, R.A.C., 2017. Mapping landslide susceptibility using data-driven methods. Sci. Total Environ. 589, 250–267.

Zhao, C., Chen, W., Wang, Q., Wu, Y., Yang, B., 2015. A comparative study of statistical index and certainty factor models in landslide susceptibility mapping: a case study for the Shangzhou District, Shaanxi Province, China. Arab. J. Geosci. 8, 9079–9088. https://doi.org/10.1007/s12517-015-1891-7.